processes

MDPI

Article

Optimization of Low-Carbon Operation in a Combined Electrical, Thermal, and Cooling Integrated Energy System with Liquid Carbon Dioxide Energy Storage and Green Certificate and Carbon Trading Mechanisms

Xiaojing Ma [1,*], Zhiqing Zhang [1], Jie Chen [2] and Ming Sun [1]

[1] College of Electrical Engineering, Xinjiang University, Ürümqi 830017, China; 107552204520@stu.xju.edu.cn (Z.Z.); sunming_xju@163.com (M.S.)
[2] College of Intelligent Manufacturing Modern Industry, Xinjiang University, Ürümqi 830017, China; xj_cj@163.com
* Correspondence: maxiaojing1983@xju.edu.cn

Abstract: The liquid carbon dioxide energy storage system (LCES), as a highly flexible, long-lasting, and environmentally friendly energy storage technology, shows great potential for application in integrated energy systems. However, research on the combined cooling, heating, and power supply using LCES in integrated energy systems is still limited. In this paper, an optimized scheduling scheme for a low-carbon economic integrated energy system is proposed, coupling LCES with power-to-gas (P2G) technology and the green certificate/carbon trading mechanism. Mathematical models and constraints for each system component are developed, and an optimization scheduling model is constructed, focusing on the economic and low-carbon operation of the integrated energy microgrid system. The objective function aims to minimize total system costs. A case study based on a northern China park is conducted, with seven scenarios set for comparative optimization analysis. The results demonstrate that the use of the combined cooling, heating, and power LCES system reduces total costs by USD 2,706.85 and carbon emissions by 34.57% compared to the single-energy flow operation. These findings validate the effectiveness of the proposed model in optimizing system costs and reducing carbon emissions.

Keywords: liquid carbon dioxide energy storage system; green certificate/carbon trading mechanism; power-to-gas; low-carbon economy

check for updates

Academic Editor: Michael C. Georgiadis

Received: 8 January 2025
Revised: 21 January 2025
Accepted: 26 January 2025
Published: 29 January 2025

Citation: Ma, X.; Zhang, Z.; Chen, J.; Sun, M. Optimization of Low-Carbon Operation in a Combined Electrical, Thermal, and Cooling Integrated Energy System with Liquid Carbon Dioxide Energy Storage and Green Certificate and Carbon Trading Mechanisms. *Processes* **2025**, *13*, 372. https://doi.org/10.3390/pr13020372

Copyright: © 2025 by the authors. Licensee MDPI, Basel, Switzerland. This article is an open access article distributed under the terms and conditions of the Creative Commons Attribution (CC BY) license (https://creativecommons.org/licenses/by/4.0/).

1. Introduction

The global push for carbon neutrality has intensified the demand for innovative solutions in energy systems. Integrated energy systems (IESs), capable of integrating electricity, heating, and cooling energy, offer significant potential for improving energy efficiency, promoting renewable energy adoption, and reducing greenhouse gas emissions [1,2]. However, the inherent intermittency of renewable energy sources and the diverse load demands of IES users present challenges to stability and efficiency [3]. These issues underscore the need for advanced energy storage technologies to enable effective energy management and support the transition to low-carbon energy systems [4].

Energy storage technologies have emerged as critical enablers of renewable energy integration and system stability [5]. Among them, liquid carbon dioxide energy storage (LCES) has drawn significant attention due to its superior performance compared to conventional storage methods like compressed air energy storage (CAES) [6,7]. LCES offers

a higher energy storage density, greater flexibility, reduced dependency on geographical conditions, and a longer operational lifespan [8].

Sun et al. [9] proposed an LCES system that uses liquid methanol and phase change materials to store sensible and latent cold energy, achieving a round-trip efficiency of 51.45% and an energy storage density of 22.21 kW·h·m^3. Wang et al. [10] developed a novel LCES system that stores cold energy in low-pressure tanks during the discharge process, with a maximum round-trip efficiency of 56.64% and an energy storage density of 36.12 kW·h·m^3. Zhao et al. [11] introduced an LCES system based on the vortex tube cooling principle, demonstrating a round-trip efficiency of 53.45% and an energy storage density of 5.43 kW·h·m^3. Recent studies indicate that LCES offers significant advantages, such as high round-trip efficiency and energy storage density, underscoring its potential in integrated energy systems. However, these studies primarily focused on the standalone economic performance of LCES, with limited exploration of its integration into multi-energy IES frameworks or its role in addressing combined cooling, heating, and power (CCHP) demands.

Jinhang Li et al. [12] proposed a dual-layer optimization model combining multiple energy storage types with IES for a low-carbon economy, showing a reduction in total operating costs by USD 122.57 and a 2.91% decrease in carbon emissions. Zhenshan Zhu et al. [13] designed an IES based on liquid air energy storage (LAES) integrated with liquefied natural gas gasification stations and power-to-gas (P2G) technology, reducing total operating costs by USD 16,646.16 and wind curtailment by 94.6%. Binxin Yin et al. [14] studied an IES combining adiabatic compressed air energy storage (AA-CAES), batteries, and P2G technology, demonstrating significant reductions in operating costs. Siyuan Huang et al. [15] proposed an optimized configuration for an LAES system coupled with combined heat and power (CHP), showing that the total economic cost could be reduced by 37.1% compared to traditional systems. Bo Li et al. [16] introduced an IES combining wind, coal-fired, and compressed air energy storage with two 600 MW coal-fired units, achieving a wind energy absorption rate of 97.72%, significantly improving renewable energy utilization. Jie Zhang et al. [17] developed an IES based on carbon capture and LCES multi-energy flow models, demonstrating improvements of 5.61%, 11.78%, and 0.71% in load rate, energy utilization, and wind-solar absorption, respectively, compared to single-energy flow systems. Additionally, Xia Wang et al. [18] proposed an IES model centered on AA-CAES, reducing the system's total operating costs by 20%. Xinglin Y et al. [19] introduced an IES combining concentrated solar power (CSP), CAES, and absorption refrigeration (AR), achieving a 59.94% reduction in total operational costs through multi-energy complementarity. However, these studies have primarily focused on the economic benefits of LCES systems, with relatively limited research on their low-carbon potential.

In the field of low-carbon research, Cailing Zhang et al. [20] proposed a low-carbon optimization scheduling strategy that incorporates flexible demand response and a tiered carbon/green certificate joint trading mechanism, reducing total costs and carbon emissions by 3.87% and 2.85%, respectively. Bin Qiu et al. [21] introduced an IES that includes a tiered carbon trading mechanism and P2G devices, reducing total operating costs and carbon emissions by 1.46% and 6.1%, respectively. Zhenbo Wei et al. [22] developed an optimization model for IES that combines carbon trading mechanisms and demand response, reducing costs by USD 1960.02 and carbon emissions by 5894.36 kg. Zhang Yi et al. [23] proposed a low-carbon economic dispatch strategy that integrates green certificate/carbon trading mechanisms with flexible cogeneration unit responses, reducing carbon trading costs by USD 631.90. Yi Tao et al. [24] proposed a demand response optimization model combining source-load coordination and a tiered carbon trading mechanism with rewards and penalties, leading to reductions in total costs and carbon emissions while enhancing peak shaving,

valley filling, and energy-saving capabilities. Jing Peng et al. [25] introduced a multi-region IES scheduling model based on a carbon–green certificate joint market, demonstrating a significant reduction in carbon emissions and a 21.5% decrease in system costs.

Analysis of the aforementioned literature reveals that energy storage systems have effectively mitigated power fluctuations in IESs, significantly improving system stability and reliability. However, most existing research has focused primarily on electricity storage, with limited attention to the integration of thermal energy, cooling energy, and other forms. While some studies have explored the role of CAES in optimizing IES capacity and operations, its advantages in combined electricity, heating, and cooling supply remain underexplored, leaving the diverse load demands of IES users insufficiently addressed. Furthermore, research on the role of LCES in optimizing IES scheduling is sparse, highlighting untapped potential in this area.

Additionally, policy mechanisms such as green certificates and carbon trading have gained prominence as effective tools for incentivizing renewable energy utilization and reducing carbon emissions. While previous studies have incorporated these mechanisms into IES optimization strategies, there remain a lack of comprehensive models that integrate LCES with these policy tools. This gap presents an opportunity to explore the synergistic effects of combining LCES with green certificate/carbon trading mechanisms, focusing on both economic and low-carbon performance.

To address these challenges, this study proposes a novel optimization framework for a low-carbon IES that integrates LCES with green certificate and carbon trading mechanisms. The contributions of this research are threefold:

- Development of a multi-energy flow optimization model: A detailed mathematical framework is introduced to optimize electricity, heat, and cooling energy flows, ensuring diverse load demands are met while minimizing costs and emissions;
- Integration of policy mechanisms: This study incorporates green certificate and carbon trading mechanisms, providing economic incentives and regulatory tools to enhance renewable energy integration and reduce carbon emissions;
- Comprehensive scenario analysis: A case study in a northern China park evaluates the effectiveness of the proposed model under multiple scenarios, demonstrating significant cost savings and carbon emission reductions.

2. Modeling of the Main Equipment of the Integrated Energy System

2.1. IES Descriptions

The IES is composed of four main components: the power supply side, the conversion side, the energy storage system, and the load side. The power supply side primarily includes the upper-level grid (PE), photovoltaic units (PV), and wind turbine units (WT). The conversion side comprises the CHP, waste heat boiler (WHB), gas boiler (GB), P2G, AR, and electric chiller (ER). The energy storage side consists of the LCES, while the load side includes electrical, thermal, and cooling loads. The ER, AR, and LCES cold storage tanks are responsible for meeting the cooling load demand, while the GB, WHB, and LCES heat storage tanks supply the thermal load. The internally generated electricity from PV, WT, and CHP units is prioritized to meet the electrical load demand, and any deficit is compensated by purchasing power from the grid, with the ER functioning as a significant power-consuming device. During periods of low load demand, the P2G system consumes excess electricity to produce natural gas, which can be sold to generate additional revenue.

To perform system performance analysis and optimize operations, mathematical models of the main components within the IES must be established, including models for LCES, P2G, CHP, WHB, GB, AR, ER, carbon trading, and green certificate trading mechanisms, as illustrated in Figure 1.

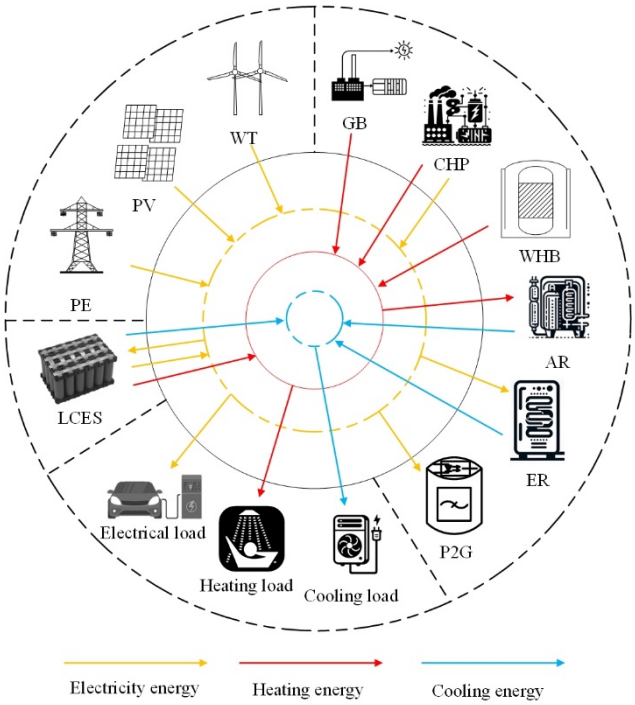


Figure 1. Integrated energy system structure diagram.

2.2. Introduction to the LCES Model

To enhance the stability and reliability of the LCES, a multi-stage compression with intercooling and multi-stage expansion with reheating operational mode is typically adopted. This approach not only improves the overall efficiency of the LCES but also enhances the system's response speed, allowing it to adjust more rapidly to fluctuations in grid load and changes in energy demand. However, approximately 40% of the compression heat in LCES systems is typically wasted. To further optimize the performance of the LCES, integrating the Kalina cycle has been identified as an effective strategy [26,27]. The Kalina cycle uses an ammonia–water mixture as the working fluid, which, due to its variable boiling point, enables better temperature matching between the hot water in the LCES heat storage tank and the ammonia–water mixture, thus improving the system's thermal efficiency. The architecture of the LCES coupled with the Kalina cycle is shown in Figure 2.

Energy Storage Process: The liquid CO_2 flowing out of the Low-Pressure liquid Storage Tank (LPST) is heated by the accumulator and then enters the three-stage compressor for compression. The heat generated during compression is absorbed by the cold water in the cold storage tank through intercooling, and the heated water is stored in a hot water tank. The cooled CO_2 is then stored in the High-Pressure liquid Storage Tank (HPST).

Energy Release Process: The liquid CO_2 in the HPST is reheated via a reheater and enters a three-stage turbine in a high-temperature and high-pressure state, driving the generator to produce electricity. Meanwhile, the heat-depleted water is stored in the cold water tank. To further improve the utilization of compression heat, the hot water is used to heat the ammonia–water mixture in a steam generator. The ammonia–water mixture then enters the turbine, driving the generator to produce additional electricity. After expansion, the CO_2 is stored in the LPST.

To simplify the model, variations in parameters such as temperature and pressure across LCES components during dynamic operating conditions are ignored. The following mathematical model for LCES is established based on this assumption [8,13,15].

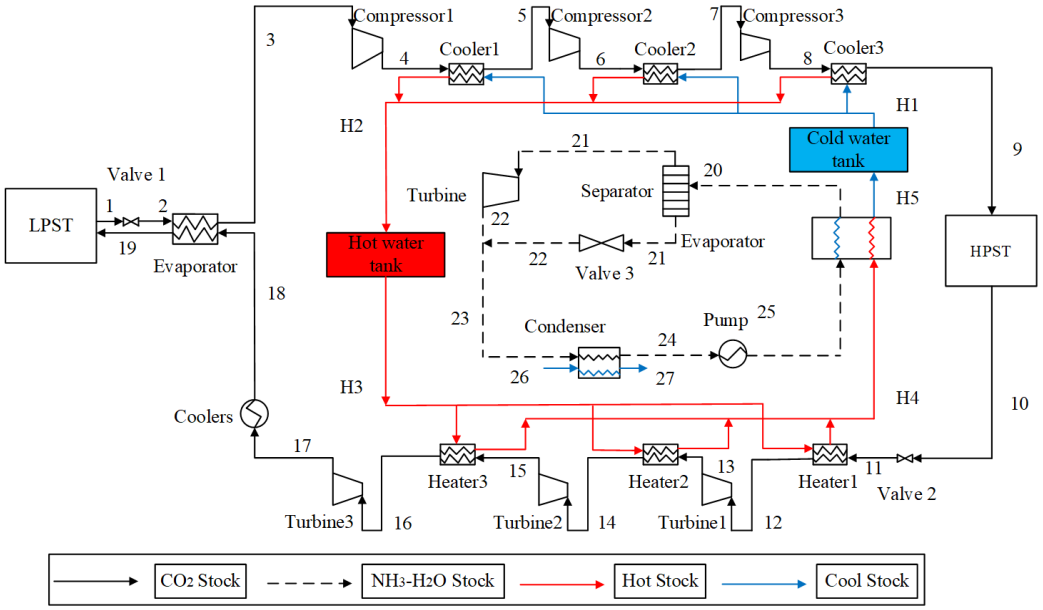


Figure 2. Diagram of the LCES-Kalina System.

Modeling of compression and expansion phases:

$$\begin{cases} P^{t}_{\mathrm{LCEScha}} = \sum_{t=1}^{n_c} \dfrac{c_{\mathrm{p}} T^{\mathrm{in}}_{\mathrm{ci}} m_c}{\eta_{\mathrm{c,m}}\eta_{\mathrm{c,ist}}\left(\lambda_{\mathrm{c}}^{\left(\frac{\beta-1}{\mathrm{n_c}\beta}\right)} - 1\right)} \\ P^{\mathrm{t}}_{\mathrm{LCESdis}} = \sum_{t=1}^{n_d} c_{\mathrm{p}} T^{\mathrm{in}}_{di} m_d \eta_{\mathrm{d,m}}\eta_{\mathrm{d,ist}}\left(1 - \lambda_d^{\left(\frac{-(\beta-1)}{\mathrm{n}_d\beta}\right)}\right) \end{cases} \tag{1}$$

where P^{t}_{LCEScha} and $P^{\mathrm{t}}_{\mathrm{LCESdis}}$ are the output power of the compressor and turbine in time period t; m_c and m_d are the mass flow rate of the mass in the compressor and turbine in time period t; β is the adiabatic index; $T^{\mathrm{in}}_{\mathrm{ci}}$ and T^{in}_{di} are the temperatures of the air entering the first stage compressor and the first stage turbine in time period t; n_c and n_d are the number of compressor and turbine stages; c_{p} is the constant pressure specific heat capacity of CO_2; $\eta_{\mathrm{c,m}}$ and $\eta_{\mathrm{d,m}}$ are the efficiency of the compressor and turbine, respectively; $\eta_{\mathrm{c,ist}}$ and $\eta_{\mathrm{d,ist}}$ are the isentropic efficiency of the compressor and turbine, respectively; and λ_{c} and λ_d are the compression ratio and expansion ratio, respectively.

The mathematical models of the high-temperature and the low-temperature water tanks are:

$$\begin{cases} H^{\mathrm{t}}_{\mathrm{HAc}} = H^{\mathrm{t}}_{\mathrm{LCESc}} - H^{\mathrm{t}}_{\mathrm{cur}} \\ H^{\mathrm{t}}_{\mathrm{HAd}} = H^{\mathrm{t}}_{\mathrm{LCESd}} + H^{\mathrm{t}}_{\mathrm{HAL}} \\ L^{\mathrm{t}}_{\mathrm{HAc}} = L^{\mathrm{t}}_{\mathrm{LCESc}} - L^{\mathrm{t}}_{\mathrm{cur}} \\ L^{\mathrm{t}}_{\mathrm{HAd}} = L^{\mathrm{t}}_{\mathrm{LCESd}} + L^{\mathrm{t}}_{\mathrm{HAL}} \end{cases} \tag{2}$$

where $H^{\mathrm{t}}_{\mathrm{HAc}}$ and $H^{\mathrm{t}}_{\mathrm{HAd}}$ are the heat storage power and heat release power of the heater in time period t; $H^{\mathrm{t}}_{\mathrm{LCESc}}$ and $H^{\mathrm{t}}_{\mathrm{LCESd}}$ are the heat of compression and heat of power generation in time period t; $H^{\mathrm{t}}_{\mathrm{cur}}$ is the amount of heat discarded by the compression process in time period t; $H^{\mathrm{t}}_{\mathrm{HAL}}$ is the power supplied to the thermal loads by the heater in time period t; $L^{\mathrm{t}}_{\mathrm{HAc}}$ and $L^{\mathrm{t}}_{\mathrm{HAd}}$ are the cooling power of the cooler in time period t; $L^{\mathrm{t}}_{\mathrm{LCESc}}$ and $L^{\mathrm{t}}_{\mathrm{LCESd}}$ are the expansion cooling capacity and compression cooling capacity in time period t; $L^{\mathrm{t}}_{\mathrm{cur}}$ is the amount of cold discarded by the expansion process in time period t; and $L^{\mathrm{t}}_{\mathrm{HAL}}$ is the power supplied to the cooling loads by the cooler in time period t.

Kalina cycle power generation process:

$$\begin{cases} Q_{EVA}^t = H_{HAL}^t = m_{EVA} c_{p,EVA} (T_{vap} - T_{evap}) \\ W_{KT}^t = \eta_{KT} \left[m_{KT} c_{p,KT} (T_{in,KT} - T_{out,KT}) \right] \\ Q_{CON}^t = m_{CON} c_{p,CON} (T_{in,CON} - T_{out,CON}) \\ W_{PUMP}^t = \frac{1}{4} m_{PUMP} \left(\frac{p_{in,PUMP}}{\rho_{in,PUMP}} - \frac{p_{out,PUMP}}{\rho_{out,PUMP}} \right) \end{cases} \tag{3}$$

where Q_{EVA}^t, W_{KT}^t, Q_{CON}^t, and W_{PUMP}^t are the power of the evaporator, the output of the Kalina turbine, the power of the condenser, and the power of the booster pump in time period t; m_{EVA}, m_{KT}, m_{CON}, and m_{PUMP} are the time-phase mass flow rates into the evaporator, Kalina turbine, condenser, and booster pump in time period t; $c_{p,EVA}$, $c_{p,KT}$, and $c_{p,CON}$ are the constant-pressure specific heat capacity of the mass entering the evaporator, Kalina turbine, and condenser; η_{KT} is the mechanical efficiency of the Kalina turbine cycle; T_{vap} and T_{evap} are the inlet and outlet temperatures of the evaporator in time period t; $T_{in,KT}$ and $T_{out,KT}$ are the inlet and outlet temperatures of the Kalina turbine in time period t; $T_{in,CON}$ and $T_{out,CON}$ are the inlet and outlet temperatures of the condenser in time period t; $p_{in,PUMP}$ and $p_{out,PUMP}$ are the booster pump mass inlet and outlet pressures in time period t; and $\rho_{in,PUMP}$ and $\rho_{out,PUMP}$ are the inlet and outlet densities of the booster pump mass in time period t.

2.3. P2G Model

The P2G system consumes excess electrical energy during periods of low user load to produce natural gas [21].

$$\begin{cases} Q_{P2G}^t = \alpha_{CO_2} \eta_{P2G} P_{P2G}^t \\ V_{P2G}^t = \frac{3.6 \eta_{P2G} P_{P2G}^t}{H_g} \end{cases} \tag{4}$$

where Q_{P2G}^t is the total amount of CO_2 consumed by P2G in time period t; α_{CO_2} is the amount of CO_2 required to generate a unit of power of natural gas and takes the value 0.2/(kg/(kWh)); η_{P2G} is the P2G conversion efficiency; P_{P2G}^t is the electric power consumed by P2G in time period t; V_{P2G}^t is the volume of natural gas generated by P2G in time period t; and H_g is the calorific value of natural gas.

2.4. CHP and WHB Models

The CHP unit and the WHB provide electrical and thermal loads for the IES through the combustion of natural gas [13].

$$P_{CHP}^t = \frac{V_{CHP}^t \eta_{CHP} H_g}{3.6} \tag{5}$$

$$H_{WHB}^t = \eta_{WHB} \left(\frac{H_g V_{CHP}^t}{3.6} - P_{CHP}^t \right) \tag{6}$$

where P_{CHP}^t is the electric power output of the CHP in time period t; V_{CHP}^t is the amount of natural gas consumed by the CHP in time period t; η_{CHP} is the electrical efficiency of the CHP; H_{WHB}^t is the heat power output of the WHB in time period t; and η_{WHB} is the waste heat recovery efficiency of the WHB.

2.5. GB Model

The GB provides the thermal load for the IES through the combustion of natural gas [20].

$$H_{GB}^t = V_{GB}^t \eta_{GB} H_g \tag{7}$$

where H_{GB}^t is the heat power output of the gas boiler (GB) in time period t; η_{GB} is the efficiency of the GB; and V_{GB}^t is the amount of natural gas consumed by the GB in time period t.

2.6. ER and AR Models

The ER provides the cooling load for the IES by consuming excess electrical energy, while the AR provides the cooling load for the IES by utilizing excess thermal energy [17].

$$L_{ER}^t = \beta_{ER} P_{ER}^t \tag{8}$$

$$L_{AR}^t = \beta_{AR} H_{AR}^t \tag{9}$$

where L_{ER}^t and L_{AR}^t are the power outputs of the ER and the AR in time period t, respectively; β_{ER} and β_{AR} are the conversion efficiencies of the ER and AR, respectively; and P_{ER}^t and H_{AR}^t are the electrical energy consumed by the ER and the thermal energy consumed by the AR in time period t, respectively.

2.7. Carbon Trading Model

The carbon trading mechanism is a tool for controlling carbon emissions by setting legally permissible carbon emission quotas and allowing producers to trade carbon emission rights on the market. Regulatory authorities allocate a certain number of carbon emission allowances to each emission source, and producers manage their production and emissions based on these allowances. If actual emissions are lower than the allocated quota, the surplus allowances can be traded on the carbon market. Conversely, if emissions exceed the quota, producers must purchase additional carbon emission allowances [22].

2.7.1. Carbon Emission Quota Model

Carbon trading mechanism as a means of controlling carbon emissions, it did so by establishing free carbon emission allowances and allow producers to trade free carbon emission quota in the market to achieve this.

$$E_{IES,M} = \tau_M(\omega_e \sum_{t=1}^{T} P_{CHP}^t + \sum_{t=1}^{T} H_{WHB}^t + \sum_{t=1}^{T} H_{GB}^t) \tag{10}$$

where $E_{IES,M}$ is the total carbon emission quota of the IES system; ω_e is the conversion factor for electricity; and τ_M is the quota of carbon emissions per unit of heat.

2.7.2. Modeling of Actual Carbon Emissions

The natural gas process of P2G absorbs a portion of CO_2, so it needs to be taken into account:

$$E_{IES,S} = \tau_S(\omega_e \sum_{t=1}^{T} P_{CHP}^t + \sum_{t=1}^{T} H_{WHB}^t + \sum_{t=1}^{T} H_{GB}^t + \omega_e \sum_{t=1}^{T} P_{P2G}^t) \tag{11}$$

where $E_{IES,S}$ is the IES system carbon emissions and τ_S is the carbon emission factor.

2.8. Green Certificate Trading Mechanism

The green certificate trading mechanism aims to promote the consumption of renewable energy by setting a minimum proportion of renewable energy generation within the electricity consumption of users. This encourages both users and power generation companies to engage in the use or sale of green electricity. Similar to the carbon trading mechanism, the green certificate trading mechanism facilitates renewable energy consumption through market transactions. When a power generation company holds more green certificates than its allocated quota, it can sell the excess certificates on the green certificate

market for profit. Conversely, if a company falls short of its quota, it must bear the cost of purchasing additional green certificates [25].

$$\begin{cases} E_{tot} = \sum_{t=1}^{T} [P_{P2G}^t + P_{LCEScha}^t - P_{LCESkalina}^t + P_{ER}^t + P_{EL}^t] \\ E_{re} = \sum_{t=1}^{T} [P_{WN}^t + P_{VN}^t] \\ E_{gc} = \varsigma(E_{re} - \psi E_{tot}) \end{cases} \tag{12}$$

where E_{tot} is the number of green certificates required by the system and the user; E_{re} is the renewable energy consumption power; E_{gc} is the number of green certificates bought/sold; ς is a quantification factor for the amount of renewable energy converted into green certificates, where one green card corresponds to 1 MW·h of renewable energy electricity; and ψ is the weight of minimum renewable electricity consumption responsibility.

3. Low-Carbon Economic Dispatch Modeling of Integrated Energy System

This paper presents a model that optimizes the operation of a combined cooling, heating, and power IES. The model not only takes into account the power balance constraints for electrical, thermal, and cooling loads but also considers the power constraints of various components, including P2G, CHP, WHB, GB, AR, ER, WT, PV, and the power exchange with the upper-level grid.

3.1. Objective Function

The collaborative optimization model of the LCES, P2G, and the green certificate/carbon trading mechanism aims to achieve the overall economic and low-carbon optimization of the IES while meeting the system constraints and user load requirements. The objective function is as follows (with costs as positive values and revenues as negative values):

$$f = \min(f_1 + f_2 + f_3 + f_4 + f_5) \tag{13}$$

where f is the total cost during the dispatch cycle; f_1 is the energy procurement cost; f_2 is the system operation and maintenance cost; f_3 is the carbon trading costs/revenues; f_4 is the system revenue; and f_5 is the green certificate trading costs/revenues.

3.1.1. Energy Procurement Cost

The energy procurement costs of the microgrid primarily consist of two components: one is the cost of natural gas consumption by the gas turbine unit, and the other is the cost of purchasing electricity from the upper-level grid.

$$f_1 = \delta_{11}(V_{CHP}^t + V_{GB}^t) + k_E^t P_E^t \tag{14}$$

where δ_{11} is the purchase price of gas and k_E^t is the purchase price of electricity using time-of-day tariffs.

3.1.2. System Operation and Maintenance Cost

Sum of operation and maintenance costs for each device:

$$f_2 = \chi_{2i} P_i^t \tag{15}$$

where P_i^t is the different equipment outputs in the system and χ_{2i} is the operation and maintenance cost coefficient.

3.1.3. Carbon Trading Costs/Revenues

To encourage active participation in the carbon trading market, users are allowed to freely trade carbon emission allowances. When a user's actual carbon emissions are lower than the allocated quota, the surplus allowances can be sold at market prices to generate economic benefits. Conversely, if actual emissions exceed the allocated quota, the user must purchase additional allowances from the market to meet emission requirements. This market-based mechanism incentivizes users to optimize their emission behavior. Costs are represented as positive values, while revenues are represented as negative values.

$$f_3 = \delta_3(E_{IES,S} - E_{IES,M}) \tag{16}$$

where δ_3 represents the carbon trading price, with a value of 0.07 USD/kg.

3.1.4. System Revenue

The sum of revenue from selling natural gas and electricity:

$$f_4 = \delta_{41} V_{P2G}^t + \delta_{42} P_{LCESkalina}^t \tag{17}$$

where δ_{41} is the price of selling gas and δ_{42} is the price of selling electricity.

3.1.5. Green Certificate Trading Costs/Revenues

It can sell the excess green certificates in the green certificate trading market to gain revenue; conversely, it needs to bear the cost of green certificate trading:

$$f_5 = \delta_5 E_{gc} \tag{18}$$

where δ_5 represents the green certificate trading price, with a value of 0.3 USD/kWh.

3.2. IES Major Equipment Constraints

3.2.1. LCES-Kalina Constraints

(1) LCES-Kalina output constraints

$$\begin{cases} P_{LCESkalina}^t = P_{\mathrm{LCESdis}}^{\mathrm{t}} - W_{PUMP}^t + W_{KT}^t \\ 0 \le P_{\mathrm{LCEScha}}^{\mathrm{t}} \le \mu_{cha}^t P_{\mathrm{LCEScha}}^{\max} \\ 0 \le P_{LCESkalina}^t \le \mu_{dis}^t P_{LCESkalina}^{\max} \\ 0 \le \mu_{cha}^t + \mu_{dis}^t \le 1 \end{cases} \tag{19}$$

where $P_{LCESkalina}^t$ is the electrical power output of the energy storage system; μ_{cha}^t and μ_{dis}^t are the charging and discharging states of the energy storage device and take the values of 0 or 1; and $P_{\mathrm{LCEScha}}^{\max}$ and $P_{LCESkalina}^{\max}$ are the maximum charging power and output power of the energy storage device in time period t.

(2) LCES-Kalina capacity constraints

$$\begin{cases} S_{ES}^t = S_{ES}^{t-1} + \left(P_{\mathrm{LCEScha}}^{\mathrm{t}} \eta_{\mathrm{cha}} + \frac{P_{LCESkalina}^t}{\eta_{\mathrm{dis}}} \right) \Delta t \\ S_{TS}^t = S_{TS}^{t-1} + \left(H_{\mathrm{HAc}}^{\mathrm{t}} \eta_{\mathrm{THAc}} + \frac{H_{\mathrm{HAd}}^{\mathrm{t}}}{\eta_{\mathrm{THAd}}} \right) \Delta t \\ S_{LS}^t = S_{LS}^{t-1} + \left(L_{\mathrm{HAc}}^{\mathrm{t}} \eta_{\mathrm{LHAc}} + \frac{L_{\mathrm{HAd}}^{\mathrm{t}}}{\eta_{\mathrm{LHAd}}} \right) \Delta t \end{cases} \tag{20}$$

$$\begin{cases} S_{ES}^{\min} \le S_{ES}^t \le S_{ES}^{\max} \\ S_{TS}^{\min} \le S_{TS}^t \le S_{TS}^{\max} \\ S_{LS}^{\min} \le S_{LS}^t \le S_{LS}^{\max} \end{cases} \tag{21}$$

where S_{ES}^t, S_{TS}^t, and S_{LS}^t are the amount of electricity, heat, and cold stored in the energy storage in time period t; η_{cha} and η_{dis} are the storage efficiency and discharge efficiency,

respectively; η_{THAc} and η_{THAd} are the heat storage efficiency and heat release efficiency of the heat accumulator, respectively; η_{LHAc} and η_{LHAd} are the cooling efficiency and cooling efficiency of the accumulator, respectively; $S_{ES}^{\min}$ and $S_{ES}^{\max}$ are the minimum and maximum storage capacity, respectively; $S_{TS}^{\min}$ and $S_{TS}^{\max}$ are the minimum and maximum heat storage capacity, respectively; and $S_{LS}^{\min}$ and $S_{LS}^{\max}$ are the minimum and maximum cooling capacity, respectively.

3.2.2. P2G Constraints

P2G upper and lower limit constraints:

$$P_{P2G}^{\min} \le P_{P2G}^{t} \le P_{P2G}^{\max} \tag{22}$$

where $P_{P2G}^{\min}$ and $P_{P2G}^{\max}$ are the upper and lower limits of the electric power consumption of the P2G device in time period t, respectively.

3.2.3. CHP and WHB Constraints

CHP and WHB upper and lower limit constraints:

$$\begin{cases} P_{CHP}^{\min} \le P_{CHP}^{t} \le P_{CHP}^{\max} \\ H_{WHB}^{\min} \le H_{WHB}^{t} \le H_{WHB}^{\max} \end{cases} \tag{23}$$

where $P_{CHP}^{\min}$ and $P_{CHP}^{\max}$ are the upper and lower limits of the electric power output of the CHP in time period t, respectively, and $H_{WHB}^{\min}$ and $H_{WHB}^{\max}$ are the upper and lower limits of the heat power output of the WHB in time period t, respectively.

3.2.4. GB Constraint

GB upper and lower limit constraints:

$$H_{GB}^{\min} \le H_{GB}^{t} \le H_{GB}^{\max} \tag{24}$$

where $H_{GB}^{\min}$ and $H_{GB}^{\max}$ are the upper and lower limits of the heat power output of the GB in time period t, respectively.

3.2.5. ER and AR Constraints

ER and AR upper and lower limit constraints:

$$\begin{cases} L_{ER}^{\min} \le L_{ER}^{t} \le L_{ER}^{\max} \\ L_{AR}^{\min} \le L_{AR}^{t} \le L_{AR}^{\max} \end{cases} \tag{25}$$

where $L_{ER}^{\min}$ and $L_{ER}^{\max}$ are the upper and lower limits of the cooling power output of the ER in time period t, respectively, and $L_{AR}^{\min}$ and $L_{AR}^{\max}$ are the upper and lower limits of the cooling power output of the AR in time period t, respectively.

3.2.6. Wind Turbine and Photovoltaic Unit Constraints

WT and PV upper and lower limit constraints:

$$\begin{cases} 0 \le P_{WN}^{t} \le P_{W}^{t} \\ 0 \le P_{VN}^{t} \le P_{V}^{t} \end{cases} \tag{26}$$

where P_{W}^{t} and P_{V}^{t} are the predicted power of WT and PV in time period t and P_{WN}^{t} and P_{VN}^{t} are the on-grid power of WT and PV in time period t.

3.2.7. Power Exchange Constraints with the Upper-Level Grid

PE upper and lower limit constraints:

$$0 \le P_E^t \le P_E^{\max} \tag{27}$$

where $P_E^{\max}$ represents the maximum electric power exchange between the microgrid and the upper-level grid in time period t.

3.2.8. Power Balance Constraints

During system operation, it must be ensured that power, heat, and cooling requirements are met, all of which need to satisfy energy balance constraints:

$$\begin{cases} P_{CHP}^t + P_{WN}^t + P_{VN}^t + P_{LCESkalina}^t + P_E^t = P_{P2G}^t + P_{LCEScha}^t + P_{ER}^t + P_{EL}^t \\ H_{WHB}^t + H_{GB}^t + H_{\mathrm{HAL}}^{\mathrm{t}} = H_{AC}^t + H_{\mathrm{HL}}^{\mathrm{t}} \\ L_{ER}^t + L_{AC}^t + L_{\mathrm{HAL}}^{\mathrm{t}} = L_{\mathrm{LL}}^{\mathrm{t}} \end{cases} \tag{28}$$

where P_{EL}^t, $H_{\mathrm{HL}}^{\mathrm{t}}$, and $L_{\mathrm{LL}}^{\mathrm{t}}$ are the electric loads, thermal loads, and cooling loads of IES users, respectively.

3.3. Model Solving Methods

The optimization scheduling model developed in this paper belongs to the category of mixed-integer nonlinear programming (MINLP). Using the Big-M method and introducing several 0–1 variables, the nonlinear terms in the model are linearized, transforming the problem into a mixed-integer linear programming (MILP) problem. The entire solution process is implemented using the YALMIP platform in MATLAB, with the CPLEX commercial solver employed for optimization.

To linearize the nonlinear terms in the nonlinear model, the specific transformation process is demonstrated using Equation (16) as an example:

$$\begin{cases} P_{LCESkalina}^t = P_{\mathrm{LCESdis}}^{\mathrm{t}} - W_{PUMP}^t + W_{KT}^t \\ 0 \le P_{\mathrm{LCEScha}}^{\mathrm{t}} \le P_{\mathrm{LCEScha}}^{\max} \\ 0 \le P_{\mathrm{LCEScha}}^{\mathrm{t}} \le \mu_{cha}^t M \\ 0 \le P_{LCESkalina}^t \le P_{LCESkalina}^{\max} \\ 0 \le P_{LCESkalina}^t \le \mu_{dis}^t M \\ 0 \le \mu_{cha}^t + \mu_{dis}^t \le 1 \end{cases} \tag{29}$$

where M is a sufficiently large constant.

The optimization model proposed in this study is implemented using the YALMIP toolbox within the MATLAB environment. YALMIP is a flexible tool for formulating and solving optimization problems, particularly for mixed-integer linear and nonlinear programming. The key steps in the implementation process are as follows:

Variable Definition: The decision variables are defined using YALMIP syntax, with both continuous and binary variables specified for the MILP model.

Objective Function and Constraints: The objective function is formulated to minimize the system cost, and the constraints are set according to the system's operational characteristics and the green certificate trading mechanism.

Solver Configuration: The CPLEX solver is employed in conjunction with YALMIP to solve the MILP problem efficiently.

4. Calculated Case Analysis

4.1. Model Setting

This paper focuses on the Hami region in Xinjiang, China, which is characterized by a relatively small population. While residential energy consumption is modest, the majority of the energy demand is driven by industrial needs. A small portion of the energy is allocated for residential use, highlighting the significant role of industrial energy consumption on the system's energy demand.

The proposed model is applied to the area to meet the electrical, thermal, and cooling load demands. The IES contains one CHP unit, one GB unit, one WHB unit, one PW unit, one PV unit, one LCES unit, one P2G unit, one ER unit, and one AR unit. The operational parameters of the LCES energy storage system are shown in Table 1. Other equipment technical parameters are shown in Table 2. The system uses time-of-day tariffs as shown in Table 3. Typical electrical, thermal, and cooling load predictions for the system are shown in Figure 3. The wind and photovoltaic power forecast output is shown in Figure 4.

Table 1. Operational parameters of LCES energy storage system.

Parameter	Value	Parameter	Value
n_c	3	n_d	3
$P^{\max}_{\mathrm{LCEScha}}/(\mathrm{kW})$	6000	$P^{\max}_{LCESkalina}/(\mathrm{kW})$	6000
λ_c	4	λ_d	3
$\eta_{\mathrm{c,m}}$	0.85	$\eta_{\mathrm{d,m}}$	0.88
$\eta_{\mathrm{c,ist}}$	0.9	$\eta_{\mathrm{d,ist}}$	0.9
$T^{\mathrm{in}}_{\mathrm{ci}}/(\mathrm{K})$	298	$T^{\mathrm{in}}_{di}/(\mathrm{K})$	384
	325		399
	330		404
η_{cha}	0.95	η_{dis}	0.95
η_{THAc}	0.92	η_{THAd}	0.92
η_{LHAc}	0.92	η_{LHAd}	0.92
$T_{vap}-T_{evap}/(\mathrm{K})$	319–400	$T_{in,KT}-T_{out,KT}/(\mathrm{K})$	400–364
$T_{in,CON}-T_{out,CON}/(\mathrm{K})$	293–320	$S^{\min}_{LS}-S^{\max}_{LS}/(\mathrm{kW})$	10–26,000
$S^{\min}_{ES}-S^{\max}_{ES}/(\mathrm{kW})$	10–10,000	$S^{\min}_{TS}-S^{\max}_{TS}/(\mathrm{kW})$	10–13,000
$p_{in,PUMP}/(\mathrm{MPa})$	1.25	$p_{out,PUMP}/(\mathrm{MPa})$	3.00

Table 2. Other equipment technical parameters.

Parameter	Value	Parameter	Value
η_{P2G}	0.6	$H_g/((\mathrm{kWh})/\mathrm{m}^3)$	9.88
η_{CHP}	0.35	η_{WHB}	0.7
η_{GB}	0.4	β_{ER}	2
$P^{\max}_{E}/(\mathrm{kW})$	10,000	β_{AR}	1.2
$P^{\min}_{P2G}-P^{\max}_{P2G}/(\mathrm{kW})$	0–4000	$L^{\min}_{ER}-L^{\max}_{ER}/(\mathrm{kW})$	0–1280
$P^{\min}_{CHP}-P^{\max}_{CHP}/(\mathrm{kW})$	0–3000	$L^{\min}_{AC}-L^{\max}_{AC}/(\mathrm{kW})$	0–640
$H^{\min}_{WHB}-H^{\max}_{WHB}/(\mathrm{kW})$	0–4500	$H^{\min}_{GB}-H^{\max}_{GB}/(\mathrm{kW})$	0–2000
$\tau_M/(\mathrm{kg}/(\mathrm{kWh}))$	0.57	ψ	0.2
$\tau_S/(\mathrm{kg}/(\mathrm{kWh}))$	0.6101	$P^{\max}_{E}/(\mathrm{kW})$	10,000
$\delta_{11}/(\mathrm{USD}/\mathrm{m}^3)$	0.34	$\delta_{41}/(\mathrm{USDm}^3)$	0.48

Table 3. Time-of-day tariffs.

Time Period	Electricity Purchase Price (USD/(kWh))	Electricity Sales Price (USD/(kWh))
01:00–07:00, 23:00–24:00	0.05	0.07
08:00–11:00, 15:00–18:00	0.09	0.07
12:00–14:00, 19:00–22:00	0.16	0.07

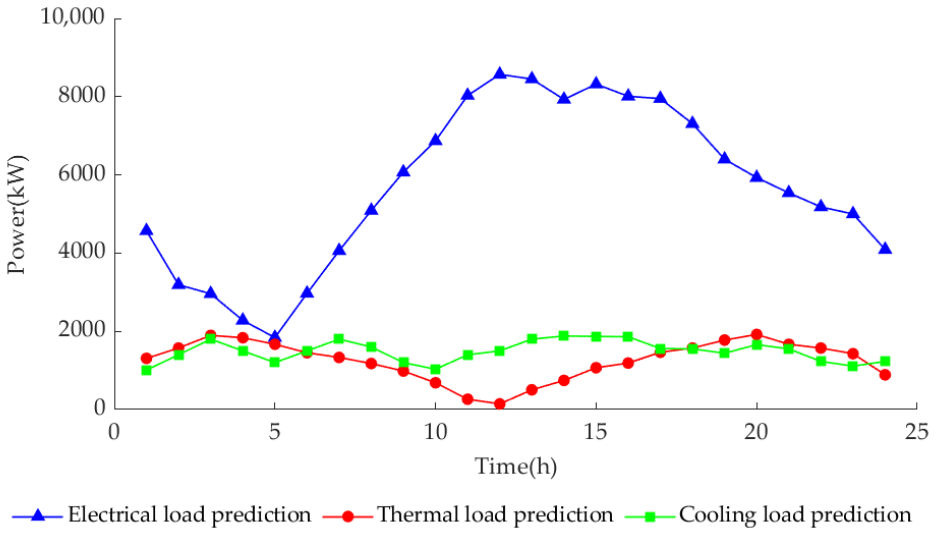


Figure 3. Forecast curves for electrical, thermal, and cooling loads.

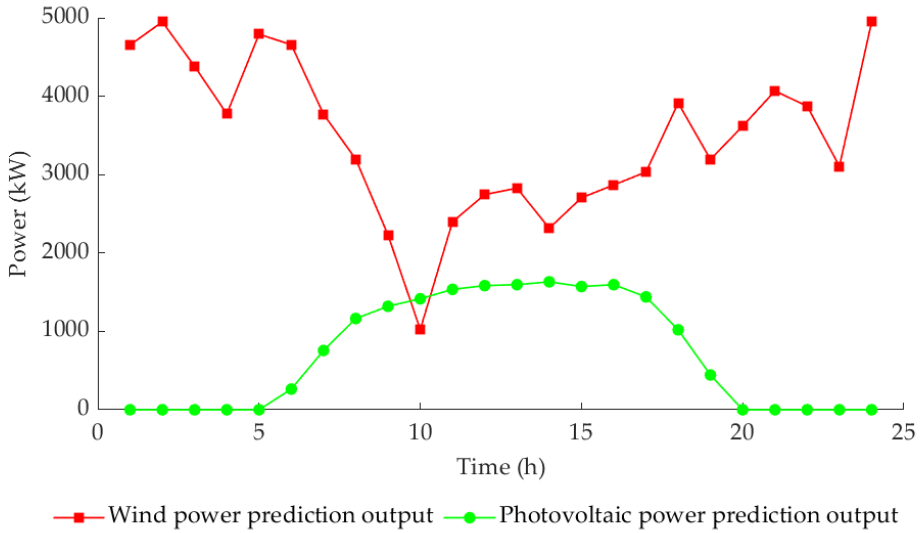


Figure 4. Wind and photovoltaic power forecast output curves.

4.2. Comparative Analysis of the Impact of LCES and P2G on IES Operational Optimization

To compare and analyze the impact of the LCES and P2G on the operational efficiency of the IES, with costs represented as positive values and revenues as negative values, this paper establishes the following four scenarios to validate the effectiveness of the proposed low-carbon economic scheduling model:

Scenario 1: Single-energy flow LCES without P2G, including carbon trading and green certificate trading;

Scenario 2: Single-energy flow LCES with P2G, including carbon trading and green certificate trading;

Scenario 3: Multi-energy flow LCES without P2G, including carbon trading and green certificate trading;

Scenario 4: Multi-energy flow LCES with P2G, including carbon trading and green certificate trading.

A comparative analysis of the cost parameters and system carbon emissions for each scenario is shown in Table 4.

Table 4. Cost comparison by scenario.

Scenario	1	2	3	4
Energy procurement cost (USD)	2434.27	2769.82	1422.17	1820.01
System operation and maintenance cost (USD)	5736.29	6105.93	3803.24	4281.20
Carbon trading costs/revenues (USD)	−175.29	−29.28	−136.36	33.88
Green certificate trading costs/revenues (USD)	−63.13	−105.85	−88.19	−134.30
Proceeds from electricity sales (USD)	−1123.52	−1246.05	−901.48	−1071.79
Proceeds from gas sales (USD)	0	−773.69	0	−899.42
Carbon footprint (kg)	80,658.72	98,094.75	52,777.29	73,497.26
Total costs (USD)	6808.61	6720.89	4101.61	4029.59

As shown in Table 4, a comparison of the costs across different scenarios reveals that Scenario 4 has the lowest total cost for the IES, while Scenario 1 exhibits the poorest economic performance. In terms of total system cost, Scenario 3, which operates the LCES in a multi-energy flow mode, reduces total system cost by USD 2706.85 and decreases carbon emissions by 34.57% compared to Scenario 1, which uses a single-energy flow LCES. This is because the multi-energy flow mode enables the LCES to provide combined cooling and heating services, resulting in greater economic benefits. A comparison between Scenarios 1 and 2 shows that the inclusion of P2G in Scenario 2 generates additional revenue from gas sales, reducing the total cost by USD 87.72 compared to Scenario 1. In the multi-energy flow mode, the introduction of P2G further reduces the system cost by USD 72.02. These findings indicate that the inclusion of LCES and P2G improves the economic performance of the system while enhancing its low-carbon characteristics.

4.3. The Impact of Green Certificate Trading and Carbon Trading Mechanisms on Microgrid System Operation Optimization

To compare and analyze the impact of green certificate trading and carbon trading mechanisms on the total cost of the IES, with costs represented as positive values and revenues as negative values, three scenarios were developed based on Scenario 4 in Section 3.2. These scenarios are used to validate the effectiveness of the proposed low-carbon economic scheduling model (Table 5).

Table 5. The impact of carbon trading and green certificate trading on the cost of IES.

Scenario	5	6	7
Energy procurement cost (USD)	6316.98	1547.87	1820.01
System operation and maintenance cost (USD)	7846.47	4026.06	4281.20
Carbon trading costs/revenues (USD)	0	−90.11	33.88
Green certificate trading costs/revenues (USD)	−232.68	0	−134.30
Proceeds from electricity sales (USD)	1071.84	−1071.79	−7841.85
Proceeds from gas sales (USD)	9048.42	−248.63	−1071.79
Carbon footprint (kg)	76,662.89	59,220.23	73,497.26
Total costs (USD)	4275.87	4163.40	4029.59

Scenario 5: Excludes carbon trading, includes green certificate trading;
Scenario 6: Includes carbon trading, excludes green certificate trading;
Scenario 7: Includes both carbon trading and green certificate trading.

A comparison between Scenario 5 through Scenario 7 shows that in Scenario5, to meet peak load demand, the IES increases the output of gas-fired equipment, leading to a sharp rise in energy procurement costs and operation and maintenance costs as well as an increase in carbon emissions. In contrast, Scenario 7 introduces the carbon trading

mechanism, where the system, constrained by carbon trading costs, reduces the output of gas-fired units such as CHP, WHB, and GB, effectively lowering carbon emissions and gas procurement costs. Additionally, the carbon trading mechanism generates extra revenue from carbon trading, further reducing the total system cost.

A comparison between Scenario 6 and Scenario 7 reveals that the introduction of the green certificate trading mechanism enhances the system's ability to consume wind power. Under this mechanism, a higher proportion of green electricity can be sold on the market, generating revenue and thereby reducing the total system cost. These results confirm the effectiveness of the green certificate trading mechanism in optimizing the system's economic performance.

Although the integration of green certificates plays a crucial role in promoting the transition to a low-carbon economy, certain limitations must be considered. Specifically, external factors, such as low-wind or low-solar insulation due to cloud cover or other conditions may prevent the system from meeting energy demand or renewable power generation targets. In such cases, fossil-fuel-based systems may need to be activated to compensate for the shortfall in renewable energy generation.

To address these limitations, the model incorporates flexibility in energy dispatch and storage. The LCES system acts as a buffer, storing excess renewable energy when available and discharging it during periods of low generation. Additionally, fossil-fuel-based backup systems are included to ensure a stable energy supply when renewable sources cannot meet demand. This approach ensures the system remains resilient and reliable, even during periods of insufficient renewable energy generation.

The following section discusses the output results of the unit operation in Scenario 4.

4.4. Analysis of Unit Output Results in Scenario 4

Based on the results obtained from optimal scheduling, Scenario 4 was selected for analysis in this paper. The electrical loads and the output of each power supply unit, the thermal loads and the output of each thermal unit, and the cooling loads and the output of each cooling unit in Scenario 4are shown in Figures 5–7. The LCES storage and discharge power and storage capacity are shown in Figure 8. Wind and photovoltaic power consumption are shown in Figure 9. The impact of different green certificate trading prices on IES is shown in Figure 10.

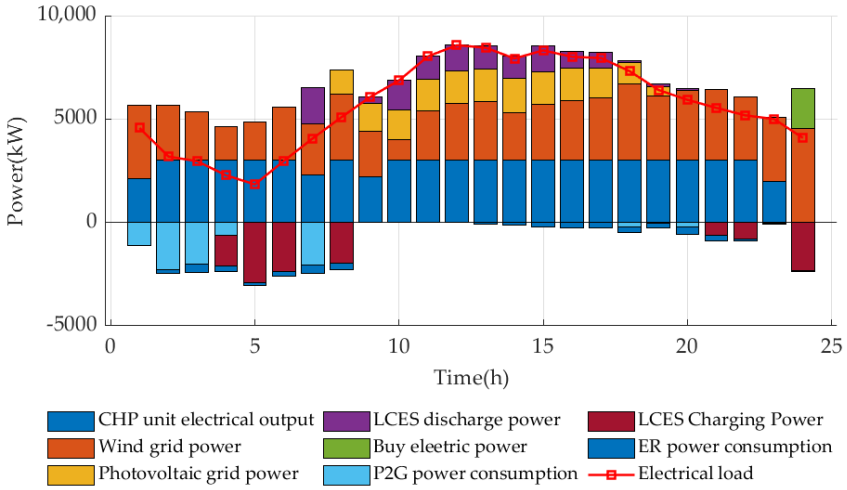


Figure 5. Electric loads and power supply unit output.

As shown in Figure 5, the electrical load demand of the power supply unit is primarily met by the CHP, PW, PV, and LCES. During peak hours from 8 a.m. to 5 p.m., the demand for electricity rises sharply. However, the CHP has limited power generation capacity, and

the LCES supplements the CHP by discharging stored energy, thereby ensuring a reliable power supply during peak periods. Outside of peak hours, when power demand decreases, the system's operation shifts. The surplus generation capacity of the CHP is better utilized, with the excess power being stored in the LCES rather than supplied directly to consumers. This ensures the system has sufficient reserve energy to meet demand during future peak periods. Additionally, during low-demand nighttime hours, the P2G system operates, converting excess electricity into natural gas, contributing additional energy to the natural gas supply system.

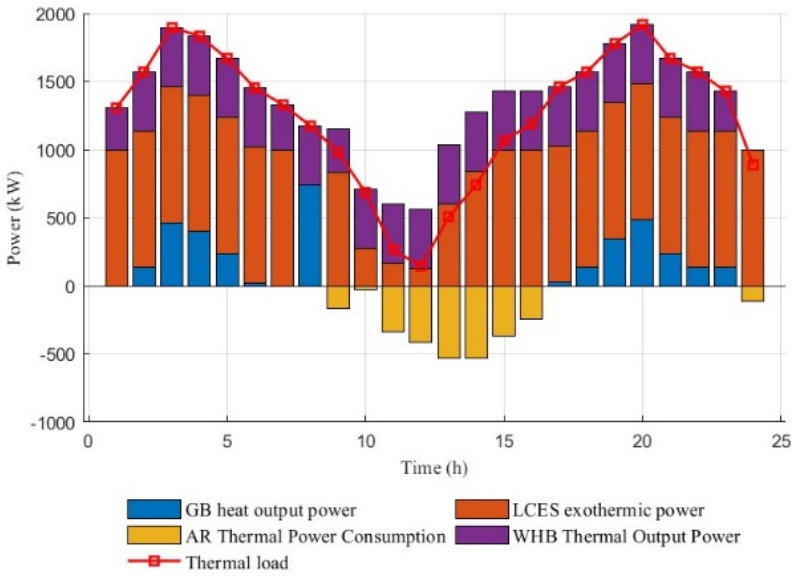


Figure 6. Thermal loads and output of each thermal unit.

As shown in Figure 6, the thermal load is primarily supplied by the WHB and the LCES. To ensure a continuous and stable electricity supply, the CHP unit must operate at high-load conditions for extended periods. During high-load operation, the waste heat generated by the CHP is recovered by the WHB, meeting the system's thermal energy demands. During periods of peak thermal load demand, the WHB plays a critical role in ensuring that the thermal requirements of the system are fully met. Additionally, the compression heat produced by the LCES serves as a key source of thermal energy. By storing excess heat generated during system operation in hot water tanks, the LCES helps maintain a stable supply of thermal energy.

Figure 7 illustrates the cooling load demand and the corresponding output of each cooling unit over a 24-h period. The cooling load is represented by the red line, while the output power from the ER, AR, and LCES systems is shown by the stacked bars. The cooling load is primarily supplied by the ER and the LCES. During nighttime low-demand periods, as the electrical load decreases, the ER utilizes excess electricity for cooling to meet the cooling load demand. During daytime peak periods, when cooling demand rises sharply, the AR becomes the primary cooling provider by utilizing thermal energy. However, the AR's cooling capacity is insufficient to fully meet peak demand, prompting the ER to activate and supplement the cooling supply by converting electricity into additional cooling energy to address peak needs. Additionally, the cold energy generated by the LCES during system operation is stored in cold water tanks, ensuring a stable cooling load supply through the stored cold energy.

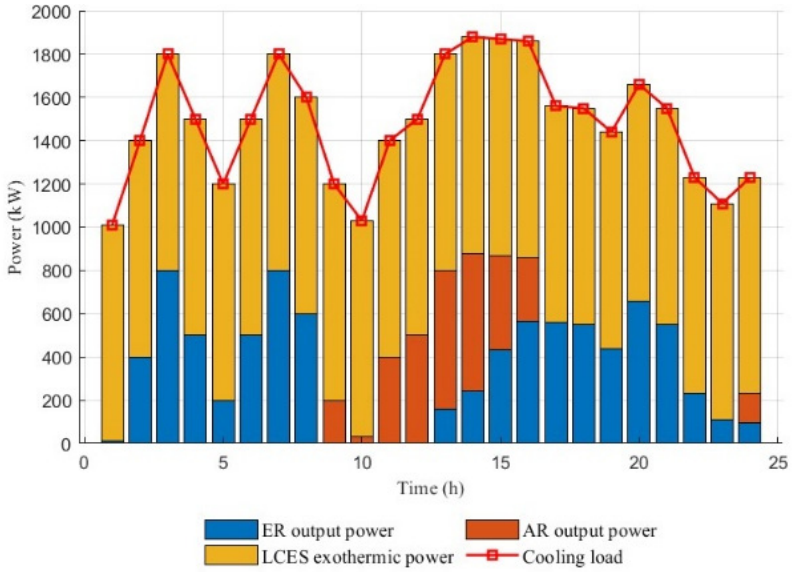


Figure 7. Cooling loads and outputs of each cooling unit.

Figure 8 illustrates the storage and discharge power of the LCES system as well as its storage capacity throughout the day. The blue bars represent the LCES charging power, and the red bars represent the LCES discharge power. The green line shows the LCES storage capacity. During periods of low electricity demand at night, the LCES compressor operates, consuming excess electricity for energy storage. During peak daytime hours, the LCES turbine is activated to drive the generator and meet the increased electricity demand. In cases where wind and PV generation experience fluctuations or unpredictability, the LCES enhances energy utilization efficiency, reducing the IES's reliance on traditional fossil fuel-based power generation.

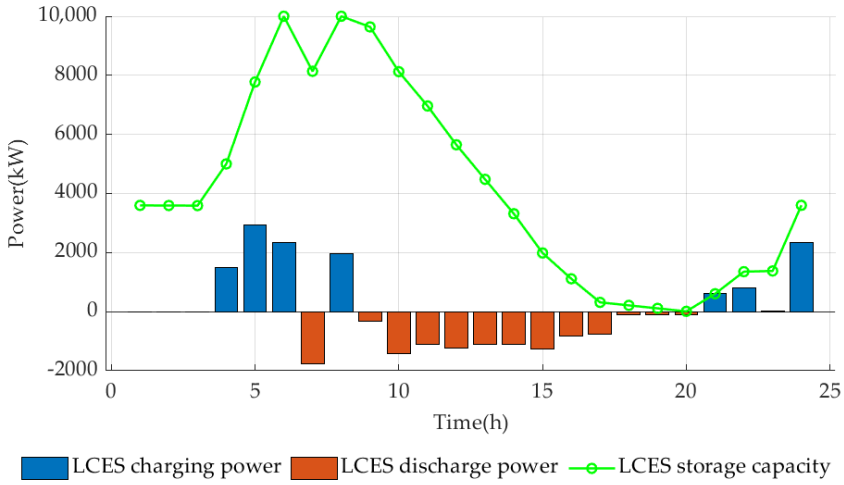


Figure 8. LCES charging and discharge power and storage capacity.

Figure 9 shows the predicted output and consumption of wind and photovoltaic power over a 24-h period. During nighttime hours when electrical load demand is lower, the LCES and P2G systems are activated to absorb excess energy from wind power. Due to the limited availability of daylight, PV power generation is primarily concentrated during periods of high electrical demand. Consequently, the consumption of renewable energy is mainly focused on the wind power generation side.

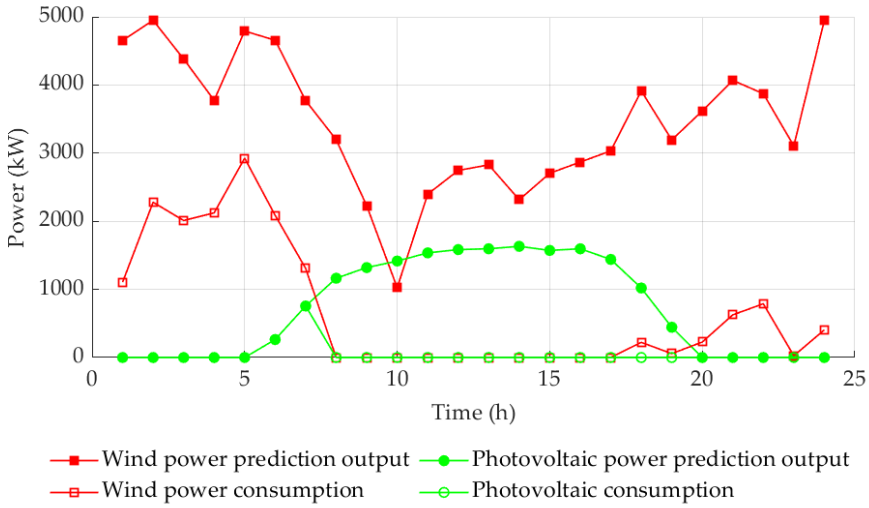


Figure 9. Wind and photovoltaic power consumption.

As shown in Figure 10, when the green certificate price is below USD 0.05, increases in the price have a minimal impact on renewable energy consumption, and the system's consumption of renewable energy remains unchanged. However, when the green certificate price ranges between USD 0.05 and 0.08, the rising cost of purchasing green certificates leads the system to reduce the number of certificates purchased, opting for alternative energy supplies, thereby decreasing the consumption of renewable energy. When the green certificate price falls within the USD 0.08 to 0.12 range, the system demand and equipment output tend to stabilize, resulting in minimal fluctuations in renewable energy consumption, which eventually remains constant. Simultaneously, as the green certificate trading price increases, the revenue from green certificates increases linearly.

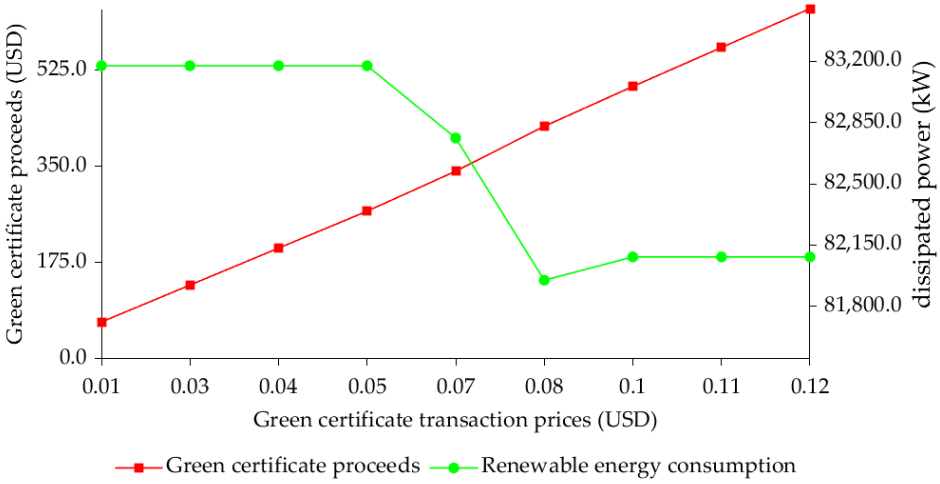


Figure 10. Impact of different green certificates trading prices on IES.

5. Conclusions

This paper focuses on a combined cooling, heating, and power microgrid IES based on an LCES. An optimization scheduling scheme is proposed, and a detailed analysis is conducted to compare the economic and low-carbon impacts of equipment such as an LCES and P2G within the IES. The entire model is solved using the YALMIP platform in MATLAB 2024 with the CPLEX solver. Five different scenarios are set to validate the proposed optimization scheme. The results demonstrate the effectiveness of the scheme in the IES, with significant improvements in both economic performance and low-carbon outcomes. Through simulation and case studies, the following conclusions were drawn:

- Economic and Low-Carbon Performance: The combined LCES and P2G system reduces total system cost by USD 2706.85 and carbon emissions by 34.57% compared to single-energy flow operation. The introduction of P2G further reduces the cost by USD 72.02. These results indicate that the combination of LCES and P2G effectively optimizes the total cost of the integrated energy system while also improving its economic efficiency and low-carbon performance.
- Impact of Green Certificates and Carbon Trading: These mechanisms facilitate the integration of renewable energy, reduce system carbon emissions, and generate dual benefits from both green certificates and carbon trading. The application of green certificate and carbon trading mechanisms reduces the total system cost by USD 133.81 and facilitates the transition to a low-carbon economy while optimizing economic performance.
- Energy Synergies: The LCES- and P2G-coupled IES optimizes the synergy between electricity, thermal, and cooling energy, successfully integrating 17.15% of wind and photovoltaic power, improving energy efficiency.

Future research could expand on this study in several key areas. First, the current model does not consider the impact of the capacities of various components within the integrated energy system (IES). Future work could explore the capacity configuration of IES, particularly with LCES, to analyze how different component capacities affect system performance and optimization. Second, the effect of electricity price fluctuations on the system was not addressed. Future studies could investigate how electricity price fluctuations influence energy scheduling and storage strategies, providing a more realistic decision-making framework under market variations. Additionally, future research could examine the role of electricity prices, green certificate policies, and carbon trading policies in optimizing economic and low-carbon performance. Regarding uncertainty, future studies could further explore how to incorporate demand fluctuations, renewable energy generation uncertainties, and market price volatility into the optimization model. Methods such as scenario analysis and sensitivity analysis could be employed to better address the challenges posed by these uncertainties. Lastly, applying the model to larger-scale, real-world integrated energy systems would test its feasibility and effectiveness in practical applications.

Author Contributions: Conceptualization, X.M. and J.C.; methodology, X.M.; software, Z.Z.; formal analysis, Z.Z.; investigation, Z.Z.; writing—original draft preparation, Z.Z.; writing—review and editing, X.M.; supervision, X.M. and M.S.; project administration, X.M.; funding acquisition, X.M. and J.C. All authors have read and agreed to the published version of the manuscript.

Funding: This research was funded by Scientific Research and Technological Development Plan of Hami High-Tech Industrial Development Zone, grant number HGX2024KJXM007, the National Natural Science Foundation of China, grant number 12362021, the Xinjiang Uygur Autonomous Region Tianshan Talent Training Program-Youth Talent Support Project, grant number 2022TSYCCX0054, and the Sponsored by Natural Science Foundation of Xinjiang Uygur Autonomous Region, grant number 2022D01C366.

Data Availability Statement: Data are contained within the article.

Conflicts of Interest: The authors declare no conflicts of interest.

References

1. Ding, S.; Lu, S.; Xu, Y. Review of cybersecurity for integrated energy systems with integration of cyber-physical systems. *Energy Convers. Econ.* **2023**, *4*, 334–345. [CrossRef]
2. Wu, N.; Zhang, F.; Wang, J. A review on modelling methods, tools and service of integrated energy systems in China. *Prog. Energy* **2023**, *5*, 3. [CrossRef]
3. Kong, D.; Jing, J.; Gu, T. Theoretical Analysis of Integrated Community Energy Systems (ICES) Considering Integrated Demand Response (IDR): A Review of the System Modelling and Optimization. *Energies* **2023**, *16*, 4129. [CrossRef]

4. Zuo, F.; Zhang, Y.; Hua, Q. Unified scheduling and configuration optimization for power to gas system considering thermal dynamics and uncertainties. *Sustain. Energy Technol. Assess.* **2024**, *64*, 103711. [CrossRef]
5. Zhuo, R.; Lu, X.; Li, H. Optimization and operational strategy analysis of steam-driven CAES systems coupled with thermal power for energy generation. *J. Energy Storage* **2025**, *108*, 114929. [CrossRef]
6. Yang, X.; Jiang, Z.; Shi, Z. Mechanical performance of polyurethane polymer mortar—A novel sealing material for CAES man-made caverns. *J. Energy Storage* **2025**, *106*, 114845. [CrossRef]
7. Chen, W.; Qin, C.; Ma, Z. Dynamic simulation and optimal design of a combined cold and power system with 10 MW compressed air energy storage and integrated refrigeration. *Energy* **2024**, *310*, 133182. [CrossRef]
8. Zeng, Z.; Ma, H.; Yang, C. Effect of the dynamic humid environment in salt caverns on their performance of compressed air energy storage: A modeling study of thermo-moisture-fluid dynamics. *Appl. Energy* **2025**, *377*, 124403. [CrossRef]
9. Sun, W.; Liu, X.; Yang, X. Design and thermodynamic performance analysis of a new liquid carbon dioxide energy storage system with low pressure stores. *Energy Convers. Manag.* **2021**, *239*, 114227. [CrossRef]
10. Wang, M.; Zhao, P.; Yang, Y. Performance analysis of energy storage system based on liquid carbon dioxide with different configurations. *Energy* **2015**, *93*, 1931–1942. [CrossRef]
11. Zhao, P.; Xu, W.; Gou, F. Performance analysis of a self-condensation compressed carbon dioxide energy storage system with vortex tube. *J. Energy Storage* **2021**, *41*, 102995. [CrossRef]
12. Li, J.; Xin, T.; Heng, C. Research on Two-layer Optimization Method for Low-carbon and Economic Operation of Integrated Energy System with Multiple Types of Energy Storage. *J. Chin. Soc. Power Eng.* **2024**, *44*, 498–508.
13. Zhen, Z.; Ming, S.; Zhe, C. Low-carbon economic dispatching of integrated energy system considering liquid air energy storage and integrated demand response. *Electr. Power Autom. Equip.* **2022**, *42*, 1–8.
14. Yin, B.; Miao, S.; Li, Y. Study on the Economic Analysis Method of Advanced Adiabatic Compressed Air Energy Storage in Integrated Energy System. *Trans. China Electrotech. Soc.* **2020**, *35*, 4062–4075.
15. Huang, S.; Wang, C.; Liang, T. Research on optimal configuration for integrated energy system with liquid air energy storage combined heat and power supply. *Energy Storage Sci. Technol.* **2024**, *13*, 1929–1939.
16. Li, B.; Shi, H. The operating characteristics research of integrated energy system based on the wind, coal-fired power plant and compressed air energy storage. *Electr. Power Technol. Environ. Prot.* **2024**, *40*, 168–177.
17. Jie, Z.; Jie, C.; Han-zhe, S. Optimal Scheduling of Integrated Energy Systems Based on Carbon Capture and Liquid CO_2 Energy Storage. *Smart Power* **2023**, *51*, 1–8.
18. Wang, X.; Ma, G.; Chen, X. Optimal Dispatch of Integrated Energy Systems Considering Advanced Adiabatic Compressed Air Energy Storage with a High Percentage of Fluctuating Energy Consumption. *J. Phys. Conf. Series. IOP Publ.* **2023**, *2659*, 012026. [CrossRef]
19. Yang, X.; Zheng, S.; Chang, J. Research on CCHP Design and Optimal Scheduling Based on Concentrating Solar Power, Compressed Air Energy Storage, and Absorption Refrigeration. *ACS Omega* **2023**, *8*, 42126–42143. [CrossRef]
20. Zhang, C.; Wang, S.; Ge, S. Integrated energy system optimization scheduling considering flexible demand response and carbon green certificate trading. *Electr. Power* **2024**, *57*, 14–25.
21. Qiu, B.; Song, S.; Wan, K. Optimal Operation of Regional Integrated Energy System Considering Demand Response and Ladder-type Carbon Trading Mechanism. *Proc. CSU-EPSA* **2022**, *34*, 87–95.
22. Wei, Z.; Ma, X.; Guo, Y. Optimized Operation of Integrated Energy System Considering Demand Response under Carbon Trading Mechanism. *Electr. Power Constr.* **2022**, *43*, 1–9.
23. Zhang, Y.; Li, L.; Hu, W. An Integrated Energy Demand Response Model Considering Source-Load Synergy and Stepped Carbon Trading Mechanism. *Eng. Lett.* **2024**, *32*, 614–624.
24. Yi, T.; Ren, W. Low carbon economy scheduling of integrated energy system considering the mutual response of supply and demand. *Sustain. Energy Grids Netw.* **2024**, *38*, 101279. [CrossRef]
25. Peng, Q.; Xu, H.; Tian, Y. A low carbon dispatching model for multiregional power systems based on carbon green certificate market mechanism. *Renew. Energy Resour.* **2024**, *42*, 1120–1126.
26. Zhang, Y.; Lin, F.; Liu, Z. Energy and exergy performance evaluation of a novel low-temperature physical energy storage system consisting of compressed CO_2 energy storage and Kalina cycle. *J. Energy Storage* **2023**, *60*, 106605. [CrossRef]
27. Zhao, P.; Wang, J.; Dai, Y. Thermodynamic analysis of an integrated energy system based on compressed air energy storage (CAES) system and Kalina cycle. *Energy Convers. Manag.* **2015**, *98*, 161–172. [CrossRef]

Disclaimer/Publisher's Note: The statements, opinions and data contained in all publications are solely those of the individual author(s) and contributor(s) and not of MDPI and/or the editor(s). MDPI and/or the editor(s) disclaim responsibility for any injury to people or property resulting from any ideas, methods, instructions or products referred to in the content.